

Supervised learning with generalized tensor networks

Ivan Glasser,¹ Nicola Pancotti,¹ and J. Ignacio Cirac¹

¹*Max-Planck-Institut für Quantenoptik, Hans-Kopfermann-Str. 1, D-85748 Garching, Germany*

Tensor networks have found a wide use in a variety of applications in physics and computer science, recently leading to both theoretical insights as well as practical algorithms in machine learning. In this work we explore the connection between tensor networks and probabilistic graphical models, and show that it motivates the definition of generalized tensor networks where information from a tensor can be copied and reused in other parts of the network. We discuss the relationship between generalized tensor network architectures used in quantum physics, such as String-Bond States and Entangled Plaquette States, and architectures commonly used in machine learning. We provide an algorithm to train these networks in a supervised learning context and show that they overcome the limitations of regular tensor networks in higher dimensions, while keeping the computation efficient. A method to combine neural networks and tensor networks as part of a common deep learning architecture is also introduced. We benchmark our algorithm for several generalized tensor network architectures on the task of classifying images and sounds, and show that they outperform previously introduced tensor network algorithms. Some of the models we consider can be realized on a quantum computer and may guide the development of near-term quantum machine learning architectures.

I. INTRODUCTION

Tensor networks, which factorize a high-order tensor into a contracted network of low-order tensors, have found a wide use of applications from quantum physics[1, 2] to machine learning[3, 4]. They can be used to compress weights of neural networks[5–8], to study model expressivity[9–13] or to parametrize complex dependencies between variables[14–17]. Recently, they have also attracted attention in the context of quantum machine learning[18, 19]: there has been much interest in understanding how low-depth quantum circuits that can be implemented on near-term quantum devices may be useful in machine learning[20–25], and tensor networks are a natural tool to perform the classical simulation of such algorithms[26, 27]. Tensor networks that can be efficiently simulated on classical computers thus provide a unique platform to benchmark and guide the development of new quantum machine learning architectures.

In this work we explore the relationship between tensor networks and more common machine learning architectures, in particular probabilistic graphical models[28–32]. We define generalized tensor networks which connect the two frameworks. These networks rely on the copy and reuse of local tensor information. Unlike regular tensor networks, they can be defined in complex geometries while remaining efficient to contract as long as an appropriate hierarchical order can be defined. We apply several variants of generalized tensor networks to image classification and environmental sound recognition and compare their performance, concluding that generalized tensor networks typically perform better than tensor networks alone. We also prove that generalized tensor networks are exponentially more efficient at describing some functions than regular tensor networks.

Generalized tensor networks share some structure with convolutional neural networks (CNN)[33, 34], while having direct connections to restricted Boltzmann machines

(RBM)[31, 35, 36]. Examples of such networks that have been used in quantum physics include String-Bond States (SBS)[37, 38], which generalize Matrix Product States (MPS) (also known as Tensor Trains[39]), as well as Entangled Plaquette States (EPS)[40–42], which can be seen as a 1-layer CNN defining all possible convolutional filters over discrete inputs. Generalized tensor networks with tree structures have also been used to study the expressivity of deep learning models[11, 43].

We introduce an algorithm for performing supervised learning with generalized tensor networks, which combines stochastic gradient descent with previously introduced approaches for tensor networks. This framework generalizes works based on regular tensor networks such as MPS[15, 16, 44, 45] or tree tensor networks[46]. It has the advantage that more complex structures can be formed while keeping the computation efficient. This is especially useful for data that possesses some geometrical structure in more than one dimension, such as images. We emphasize that the algorithm does not need to rely on any Monte Carlo techniques. This is unlike in quantum physics, where generalized tensor networks can only be optimized in combination with computationally expensive Monte Carlo sampling. In particular the cost of optimizing a SBS is only a constant factor times the cost of optimizing a MPS, but SBS are much more flexible in higher dimensions and can interpolate between a MPS and a restricted Boltzmann machine.

We discuss how real-valued data can be used in conjunction with tensor networks and suggest to learn the relevant tensor features of real data as part of the network. Inspired by deep network architectures, we also propose two ideas to combine neural networks and tensor networks. In the first case we use a neural network to extract features from the data in order to feed them into a tensor network, in the second we combine generalized tensor networks and neural networks in the same deep network architecture.

We benchmark our algorithms for several generalized tensor network architectures on different datasets[47–49]. For image classification, we find that generalized tensor networks outperform previously introduced tensor network algorithms based on MPS or trees while keeping a small dimension of the tensors. In the context of environmental sound recognition, we find that MPS and SBS deliver comparable performance. This shows that SBS should also be considered along with MPS when considering one-dimensional data, especially in the presence of long-range correlations, and may be applied in other settings such as natural language processing.

Some of the architectures we consider can be realized on a quantum computer, and serve as a reminder that the copy of classical input data may also be useful in quantum machine learning algorithms that cannot be simulated classically.

II. GRAPHICAL MODELS AND GENERALIZED TENSOR NETWORKS

We first review definitions of probabilistic graphical models and tensor networks, discuss their relationship and show that the two frameworks can be connected through the definition of generalized tensor networks in which parts of the network can be copied and reused. Examples of generalized tensor networks which have been successfully used in quantum physics are introduced, and their connection to more common machine learning architectures is discussed. It is also proven that generalized tensor networks can represent some functions with exponentially fewer parameters than regular tensor networks.

A. Graphical models

Let us consider a set of discrete random variables $\mathbf{X} = \{X_1, \dots, X_N\}$ taking values $\mathbf{x} = (x_1, \dots, x_N)$ and a dataset of samples from these variables $\mathcal{D} = \{\mathbf{d}_1, \dots, \mathbf{d}_{|\mathcal{D}|}\}$. Inferring the underlying probability distribution $p(\mathbf{x})$ can be done by maximizing the log-likelihood

$$\mathcal{L} = \sum_{i=1}^{|\mathcal{D}|} \log p(\mathbf{d}_i). \quad (1)$$

A common choice of parametrized models for p are graphical models[50], which correspond to a factorization of the probability distribution over a graph. Consider a graph $G = (V, E)$, where V is a set of vertices, E a set of edges between these vertices (each $e \in E$ is a pair of elements in V) and $\text{cl}(G)$ is the set of maximal cliques of the graph. An undirected graphical model or a Markov random field defines a factorization of the joint probability of all random variables as

$$p(\mathbf{X} = \mathbf{x}) = \frac{1}{Z} \prod_{C \in \text{cl}(G)} \phi_C(\mathbf{x}_C), \quad (2)$$

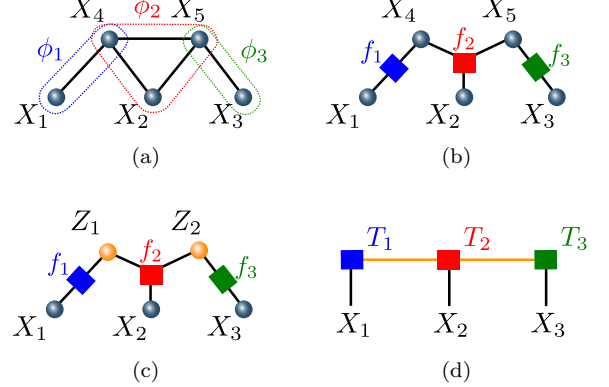


FIG. 1. (a) Undirected graphical model with three maximal cliques depicted in colors (b) Corresponding factor graph (c) Factor graph with hidden units in orange that are marginalized (d) Equivalent tensor network, which is a Matrix Product State.

where \mathbf{x}_C are the values of the random variables in clique C , ϕ_C are the clique potentials which are positive functions and Z is the partition function that ensures normalization of the probability (Fig. 1a). Graphical models can be converted to factor graphs[51] defined on a bipartite graph of factors and variable vertices: one factor node f_s is created for each maximal clique and the factor is connected to the variables in the corresponding clique (Fig. 1b). The factorization of the probability distribution still reads

$$p(\mathbf{X} = \mathbf{x}) = \frac{1}{Z} \prod_s f_s(\mathbf{x}_c), \quad (3)$$

and inference can be performed through belief propagation and the sum-product algorithm on factor graphs. To increase the set of distributions which can be represented we can add additional dependencies by introducing ancillary hidden variables (which are unobserved, i.e. their values are not supplied in the data) $\mathbf{Z} = \{Z_1, \dots, Z_M\}$ (Fig. 1c). The resulting probability distribution is obtained by marginalizing these hidden variables:

$$p(\mathbf{X} = \mathbf{x}) = \frac{1}{Z} \sum_{\mathbf{z}} \prod_s f_s(\mathbf{x}_c, \mathbf{z}_c). \quad (4)$$

B. Tensor networks and graphical models duality

We now consider a graph $G = (V, E)$ where some of the edges represent open legs containing only one vertex. We denote E' the subset of E containing edges that connect two vertices. We associate an integer size D_e called the bond dimension to each edge and define a tensor $T_v \in \otimes_{e \in v} \mathbb{R}^{D_e}$ for each vertex $v \in V$, with indices associated with the edges of this vertex. A tensor network state is

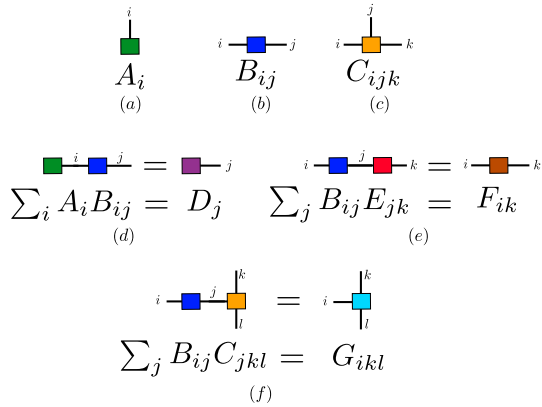


FIG. 2. Graphical notation for tensor networks : (a) vector, (b) matrix, (c) order 3 tensor, (d) vector-matrix multiplication (e) matrix-matrix multiplication (f) matrix-tensor contraction.

defined by contracting indices along all edges in the graph that connect two tensors (see Fig. 2 for an introduction to the graphical notation of tensor networks). The resulting tensor network is a tensor indexed by the indices of the open legs, denoted as x_i :

$$T_{\mathbf{x}} = \sum_{e \in E'} \prod_v T_v. \quad (5)$$

A particular case are one-dimensional Matrix Product States (MPS) (Fig. 1d), also known as tensor trains[39], which decompose a tensor as

$$T_{x_1, \dots, x_N} = \sum_{e \in E'} A_{e_1}^{x_1} A_{e_2, e_3}^{x_2} A_{e_3, e_4}^{x_3} \cdots A_{e_N}^{x_N}, \quad (6)$$

where, for fixed value of \mathbf{x} , A^{x_1} and A^{x_N} are vectors, and A^{x_j} , $j = 2, \dots, N-1$ are matrices. On a closed chain (also known as tensor ring[52]), the corresponding decomposition is

$$T_{x_1, \dots, x_N} = \text{Tr} \left(\prod_{j=1, \dots, N} A^{x_j} \right), \quad (7)$$

where all A^{x_j} are matrices. Generalizations to trees and lattices in higher dimensions have also been studied.

If we now look back at the definition of factor graphs and in the case where all variables are discrete, the factors are tensors with legs connecting to the variables. Marginalization of a hidden variable corresponds to contracting the indices of the different factors connected to this variable. Tensor networks are therefore factor graphs where all variables connected to at least two factors are hidden, and the open legs correspond to visible variables (Fig. 1c and 1d). This connection has been previously observed in Refs.[28–31] in particular models, and we refer to Ref. [32] for a more detailed analysis of this duality. An important difference remains: tensors of a factor graph coming from a graphical model have non-negative

elements, while tensor networks are usually studied in the context of real (or complex) elements. Despite the similar structure, this has important consequences for the optimization algorithms. Graphical models can be used in conjunction with expectation-maximization algorithms, which rely on the computation of conditional probabilities of some of the variables. Tensor network do not have a probabilistic interpretation of the hidden variables, but powerful optimization algorithms such as the Density Matrix Renormalization Group (DMRG) can rely on the singular-value decomposition of matrices.

C. Generalized tensor networks

It is interesting to note that there are simple classes of graphical models which do not share the properties of tensor networks that all visible variables are only connected to one factor. An example are Restricted Boltzmann Machines (RBM)[35, 36], which are defined on a bipartite graph with visible variables \mathbf{X} and hidden variables \mathbf{H} (Fig. 4a). The connections between variables on this graph take the form of Ising interaction and the probability distribution of joint variables is

$$p(\mathbf{x}, \mathbf{h}) = \frac{1}{Z} e^{\mathcal{H}(\mathbf{x}, \mathbf{h})}, \quad (8)$$

where the Hamiltonian \mathcal{H} is a classical Ising Hamiltonian defined as (we omit here the bias terms for simplicity)

$$\mathcal{H} = \sum_{i,j} w_{ij} h_i x_j.$$

In the case where both visible and hidden variables are binary valued, the resulting probability distribution once the hidden variables have been marginalized is

$$P(\mathbf{x}) = \frac{1}{Z} \sum_{\mathbf{h}} e^{\mathcal{H}(\mathbf{x}, \mathbf{h})}, \quad (9)$$

$$= \frac{1}{Z} \prod_i (1 + e^{\sum_j w_{ij} x_j}). \quad (10)$$

Seen as a tensor network, the RBM is defined on a graph with loops, but can still be contracted efficiently and $p(\mathbf{x})$ or $p(\mathbf{h}|\mathbf{x})$ can be computed analytically for arbitrary sizes. This relies on the fact that once we fix the value of the visible variables, the contraction of the network from bottom to top becomes efficient.

This leads us to the definition of a new class of tensor networks, that we call generalized tensor networks, where the value of tensors can be copied and reused in different parts of the network. As long as the remaining parts of the networks are efficiently contractible, the tensor network can still be contracted assuming the visible variables to be fixed. We graphically depict this through a red dot between edges of the graph and an arrow which marks the incoming edge. This copy operation copies vector inputs, resulting in two copies of the original vector

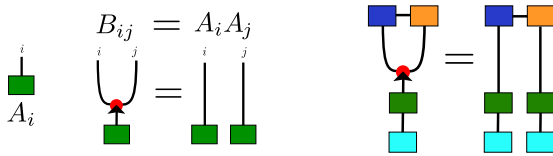


FIG. 3. Copy operation of a vector input A_i , resulting in a new tensor $B_{ij} = A_i A_j$, or of a tensor network.

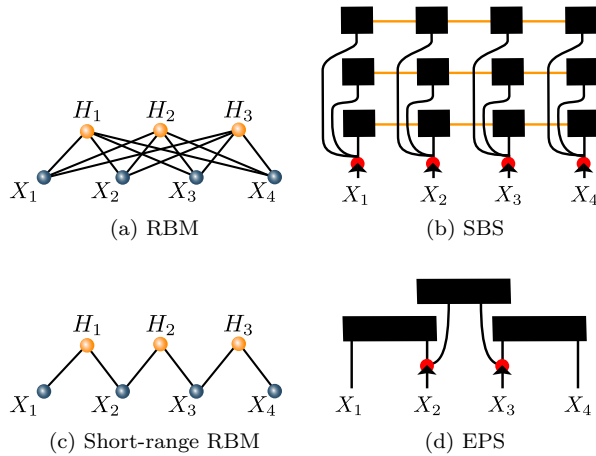


FIG. 4. (a) Restricted Boltzmann Machine (RBM) consisting of visible and hidden variables (b) String-Bond State with 1D geometry generalizing RBM. The legs corresponding to contracted indices in each MPS are depicted in orange for visibility. (c) Short-range RBM with local connections between visible and hidden variables (d) Entangled Plaquette State (EPS) generalizing the short-range RBM.

(Fig. 3). More generally one can apply this copy operation to a larger tensor network, which is then copied. In practice one would first contract the incoming network, resulting in a vector. This vector is then copied and sent to the remaining edges. The rest of the tensor network can then be independently contracted. We impose that there are no directed loops containing dots and ensure that the tensor network can be efficiently contracted as long as it is contracted in the right order.

In general, it is not possible to write this dot as a tensor[43]. In particular cases, when all the inputs are discrete and in a fixed basis, it is possible to write the copy operation as a COPY-dot tensor, as introduced in Ref.[53]. For discrete inputs and when the copy operation only applies to the inputs, the generalized tensor network can therefore be written as a tensor network including COPY-dot tensors. In the more general case, while it is not possible to represent the copy operation as a tensor, duplicating a vector and sending it to two different parts of the calculation is easily achieved in practice. The generalized tensor network can in this case be viewed as a larger tensor network containing several copies of the same tensors (weight sharing) and with inputs which are copied several times.

Examples of such tensor networks with copy of the input states have been used in the quantum physics community. The simplest example are Entangled Plaquette States (EPS)[40–42], also known as Correlator Product States, in which the tensor network is defined as a product of smaller tensors on overlapping clusters of variables:

$$T_{x_1, \dots, x_N} = \prod_{p=1}^P T_p^{\mathbf{x}_p}, \quad (11)$$

where a coefficient $T_p^{\mathbf{x}_p}$ is assigned to each of the 2^{n_p} (for binary variables) configurations \mathbf{x}_p of the variables in cluster p . Because the clusters overlap, the value of each variable is copied to all the tensors in which it is included. A sparse or short-range RBM is a special case of EPS[31] (eventually non-local for a sparse but non-local RBM) in which the tensor $T_p^{\mathbf{x}_p}$ takes the particular form $(1 + e^{\sum_j w_{pj} x_j})$, where the sum is limited to the variables in each cluster. EPS also share some similarity with Convolutional Neural Networks (CNN): a convolutional layer with discrete inputs is a particular case of EPS with weight sharing between the tensors. The EPS realizes all possible convolutional filters over a discrete input space, instead of selecting a small number of filters as CNN do.

Another example are String-Bond States (SBS)[37, 38], defined by placing Matrix Product States over strings (each string s is an ordered subset of the set of variables) on a graph which need not be a one-dimensional lattice. The resulting tensor network is

$$T_{x_1, \dots, x_N} = \prod_s \text{Tr} \left(\prod_{j \in s} A_{s,j}^{x_j} \right). \quad (12)$$

The value of each visible variable is copied and sent to different MPS. A RBM is a special case of SBS[31] for which each string is associated with a hidden variable and covers all visible variables, and the matrices are taken to be

$$A_{s,j}^{x_j} = \begin{pmatrix} 1 & 0 \\ 0 & e^{w_{sj} x_j} \end{pmatrix}. \quad (13)$$

SBS thus provide a generalization of RBM that is naturally defined for discrete variables of any dimension and can introduce different correlations through the use of higher dimensional and non-commuting matrices. Since SBS also include a MPS as a particular case, they provide a way to interpolate between a MPS (large bond dimension, only one string) and a RBM (bond dimension 2, diagonal matrices, many strings). Different choices of string geometries can be used and the geometry may be defined depending on the problem. For example in 2 dimensions (which is more suitable to images), one may place only short horizontal and vertical strings covering the 2D lattice (Fig. 5a). We will denote this kind of SBS as 2D-SBS. Correlations along one of the two dimensions can be captured in the corresponding MPS, and more complex correlations are included through the overlap of

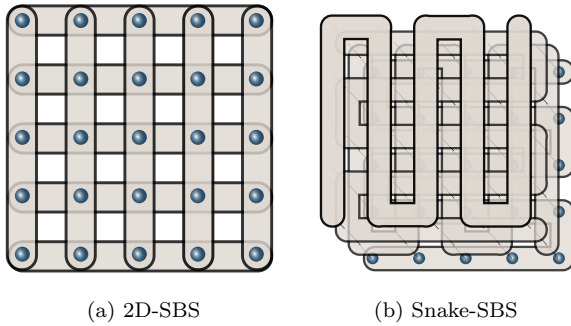


FIG. 5. Possible geometries of SBS: (a) 2D-SBS consisting of horizontal and vertical overlapping strings. (b) Snake-SBS consisting of 4 overlapping strings in a snake pattern.

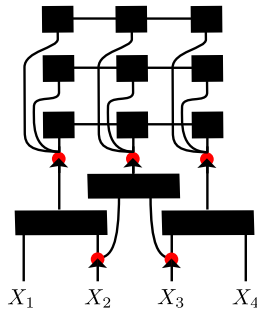


FIG. 6. EPS-SBS consisting of a first layer of EPS, followed by a copy operation and a second layer of SBS.

the different strings. We also consider the choice of 4 strings, each covering the whole lattice in a snake pattern, but in a different order (Fig. 5b). We denote these SBS as snake-SBS. They have the advantage, compared to a MPS, that two nearest neighbours variables always appear next to each other in one of the 4 strings, thus rendering the capture of strong local correlations efficient. More complex string geometries can be considered, and the choice of string could be itself learned with a RBM.

More generally, one can think of complex networks built using the copy operation for gluing different networks together. As example we will later consider the case of an EPS, whose output are copied and taken as input into a SBS (Fig. 6). The input variables are first copied and fed into overlapping clusters parametrized by tensors. The output leg of each of these tensors is a vector which is copied a few times. Each of these copies can then be contracted with the open legs of a different MPS, forming together a SBS. In 2D, we choose 2x2 overlapping plaquettes in the first layer, and 4 strings forming a snake-SBS in the second layer. In the following we will call this generalized tensor network EPS-SBS, but we observe that more complex networks based on trees or hierarchical designs with more than two layers can also be constructed in the same way.

These generalized tensor networks have the advantage, compared to standard tensor networks, that they can be

easily defined in arbitrary dimension and geometry while remaining efficient to contract, as long as the input is fixed. This is in contrast to a 2D tensor network previously introduced in physics known as Projected Entangled Pair States[54], which is naturally defined in higher dimensions, but cannot be contracted exactly efficiently. 2D-SBS form a subclass of Projected Entangled Pair States that remains efficient to contract. Moreover, the reuse of input information in generalized tensor network is more similar to state-of-the-art CNN, and weights can also be shared between different tensors.

D. Expressivity of generalized tensor networks

Another advantage of generalized tensor networks is that they can represent some functions with exponentially fewer parameters than regular tensor networks. To show this, let us consider N discrete variables $\mathbf{x} = (x_1, \dots, x_N)$ and a function $f(\mathbf{x})$. To study correlations between the variables, we define two different subsets of the variables A ($\mathbf{x}_A = (x_1, \dots, x_M)$) and B and ($\mathbf{x}_B = (x_{M+1}, \dots, x_N)$) and consider the matrix

$$\Psi_{ij} = f(\{\mathbf{x}_A^i, \mathbf{x}_B^j\}), \quad (14)$$

where \mathbf{x}_A^i denotes the possible configurations of vector \mathbf{x}_A . The entanglement entropy of subsystem A is defined as the Von Neumann entropy of the matrix $\Psi\Psi^\dagger$, that is $S_A(f) = -\sum_a s_a \log s_a$, where s_a are the eigenvalues of $\Psi\Psi^\dagger$ (where f is normalized such that $\sum_a s_a = 1$). Regular tensor network functions have the property, known as area law[2], that S_A is bounded by $k \log D$, where k is the number of edges in the network cut when bipartitioning the system into systems A and B , and D is the bond dimension of these edges. For a MPS on an open chain, this means that if A consists of the first M variables, then $S_A \leq \log D$. This statement shows that tensor network can represent only very particular functions efficiently. If $S_A(f)$ scales as the number of variables in A (which is generically the case for a random function), then it cannot be represented by a regular tensor network such as a MPS or a tree tensor network unless D scales exponentially with N .

Let us show that generalized tensor networks do not suffer from the same limitations. We consider the function, defined for binary variables on an open chain x_1, \dots, x_N with N even,

$$f(\mathbf{x}) = \prod_{l=1}^{N/2} g(x_l, x_{N-l+1}), \quad (15)$$

where $g(x_i, x_j) = \frac{1}{\sqrt{2}}(-1)^{x_i} \text{XOR}(x_i, x_j)$, which as a matrix, in the basis (x_i, x_j) , takes the form

$$g = \sqrt{\frac{1}{2}} \begin{bmatrix} 0 & 1 \\ -1 & 0 \end{bmatrix}. \quad (16)$$

g is a function of only two variables, so can be represented exactly by a tensor over these two variables which can also be written as a MPS of bond dimension 2. The product structure of f is the same as the product structure of an EPS or a SBS, so an EPS with $N/2$ plaquettes consisting of the corresponding pairs of spins, or a SBS with $N/2$ strings of length two over these pairs, can represent f exactly. Moreover a SBS with $N/2$ strings over the whole chain (Fig. 4b) can also represent f by using identity matrices in each string for all except two variables. This shows that f can be represented exactly with generalized tensor networks with a number of parameters scaling polynomially in N .

Let us now show that this function cannot be represented by a regular local tensor network defined on this open chain. We consider the subsystem A of the first $N/2$ variables, and B of the remaining $N/2$ variables and compute $S_A(f)$. Let us define a new basis $\mathbf{x}'_B = (x_N, \dots, x_{N/2+1})$ for subsystem B. In the basis formed by vectors $\{\mathbf{x}_A, \mathbf{x}'_B\}$, Ψ takes the form

$$\Psi = \bigotimes_{\ell=1}^{N/2} \sqrt{\frac{1}{2}} \begin{bmatrix} 0 & 1 \\ -1 & 0 \end{bmatrix}, \quad (17)$$

hence $\Psi\Psi^\dagger$ is diagonal and proportional to the identity matrix : $\Psi\Psi^\dagger = \frac{1}{2^{N/2}} \mathbb{1}$. The entanglement entropy can be computed as

$$S_A(f) = - \sum_{a=1}^{2^{N/2}} \frac{1}{2^{N/2}} \log \left(\frac{1}{2^{N/2}} \right) = \frac{N}{2} \log(2). \quad (18)$$

Because $S_A(f)$ scales as N , a regular tensor network such as a MPS or a tree tensor network representing f would need a bond dimension exponential in the system size, hence an exponential number of parameters.

III. SUPERVISED LEARNING ALGORITHM

Graphical models are usually used in conjunction with unsupervised learning algorithms, since they are designed to represent probability distributions. In particular cases it is possible to compute the normalization Z , which gives exact access to the likelihood and makes maximum likelihood estimation tractable. This is possible for graphical models and tensor networks on trees and has led to an algorithm for unsupervised learning with MPS[44]. In the more general case, which includes RBM, the normalization Z cannot be computed efficiently. Approximate algorithms relying on Monte Carlo sampling can then be used, such as contrastive divergence[36, 55]. Generalized tensor networks suffer from the same issue, which makes unsupervised learning computationally expensive. Since these networks correspond to quantum states, it might be possible to implement them on a quantum computer and sample from them efficiently. In this work we focus instead on supervised learning, where access to the normalization Z is not necessary. In this section we discuss

how RBM can be used for supervised learning, and generalize the corresponding algorithm to generalized tensor networks.

A. Supervised learning with Restricted Boltzmann Machines

We first review how RBM can be used to perform supervised learning, in a classification setting[56, 57]. Given labelled training data $\mathcal{D} = \{(\mathbf{x}_i, y_i)\}$, where the y_i take discrete values corresponding to different classes, a RBM can be used to approximate the joint probability distribution of the variables and labels:

$$p(\mathbf{x}, y) = \frac{1}{Z} \sum_{\mathbf{h}} e^{\mathcal{H}(\mathbf{x}, \mathbf{h}, y)} \quad (19)$$

In such a model, the label is seen as an additional visible variable (Fig. 7a), possibly encoded in a one-hot representation to use only binary units. Training such a generative model can be done by maximizing the likelihood (Eq.(1)). Since the likelihood is intractable, because the partition function Z cannot be efficiently computed, such a training can be done through approximate algorithms such as contrastive divergence. In supervised learning, one is interested in computing the conditional distribution

$$p(y|\mathbf{x}) = \frac{p(\mathbf{x}, y)}{\sum_{y_j} p(\mathbf{x}, y_j)}, \quad (20)$$

which can be computed analytically when the number of classes is small enough, since the two partition functions in Eq. 20 cancel. The label predicted by the model for new data \mathbf{x}_i is the label maximizing $p(y|\mathbf{x}_i)$. Since one is ultimately interested in classification performance, it can be advantageous to directly optimize $p(y_i|\mathbf{x}_i)$, which leads to a cost function to minimize

$$\mathcal{L}_{\text{discriminative}} = - \sum_{i=1}^{|D|} \log p(y_i|\mathbf{x}_i), \quad (21)$$

whose gradient can be computed analytically. In this setting the discriminative RBM can be seen as a single layer neural network, with a special structure of weight sharing for different fixed outputs and cross-entropy loss function. A RBM can moreover be trained in a semi-supervised way, by using a combination of discriminative and generative training.

B. Supervised learning with generalized tensor networks

To generalize the discriminative training of RBM to generalized tensor networks, we approximate the joint

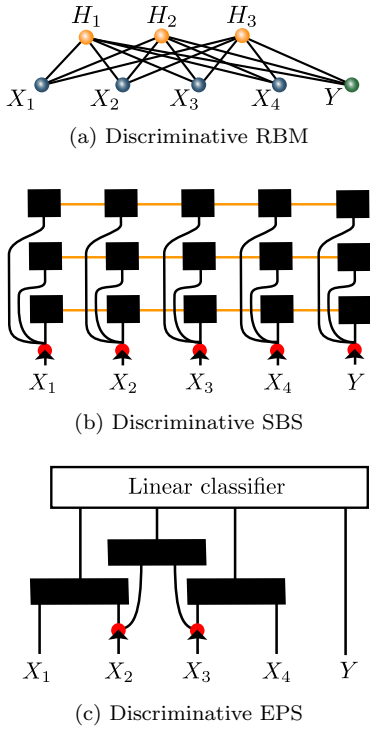


FIG. 7. (a) A classification RBM turns the label into an additional visible unit. (b) The same procedure can be defined for a SBS by adding a node corresponding to the label, and corresponding tensors which connect it to the rest of the tensor network. (c) Generalized tensor networks can be combined with additional layers of neural networks. For example an EPS output is a tensor that can be combined with a linear classifier.

probability distribution of the variables and labels as a tensor network:

$$p(\mathbf{x}, y) \propto \text{GTN}(\mathbf{x}, y), \quad (22)$$

where $\text{GTN}(\mathbf{x}, y)$ is the function resulting of the contraction of a generalized tensor network. The label is now seen as the index of one tensor. Since it is discrete, there is no need to use a one-hot representation and one can simply enlarge the dimension of the leg of a tensor to accommodate for the number of possible classes. For generalized tensor networks, once the network inputs are fixed, the network factorizes in several tensor networks in the last layer. Each of these tensor networks can have a tensor indexed by the label (Fig. 7b). We then define

$$\text{GTN}(y_k | \mathbf{x}_i) = \frac{\text{GTN}(\mathbf{x}_i, y_k)}{\sum_{y_j} \text{GTN}(\mathbf{x}_i, y_j)}, \quad (23)$$

the cost function is again chosen to be a cross-entropy loss (Eq. (21)) and it can be optimized using stochastic gradient descent, since its gradient over a small batch of

training examples can be expressed using

$$\begin{aligned} \frac{\partial \log \text{GTN}(y_i | \mathbf{x}_i)}{\partial w} &= \frac{\partial \log \text{GTN}(\mathbf{x}_i, y_i)}{\partial w} \\ &\quad - \sum_{y_j} \text{GTN}(y_j | \mathbf{x}_i) \frac{\partial \log \text{GTN}(\mathbf{x}_i, y_j)}{\partial w}. \end{aligned} \quad (24)$$

$\text{GTN}(\mathbf{x}_i, y_j)$ can be computed exactly by fixing the value of the input units and labels and contracting the network, as long as each of the tensor networks separated by copy operations can be efficiently contracted. We note that in general we can contract the whole network without the labels, and perform the contraction for the different labels as a last step. Contraction of the whole network for different labels thus only adds a small cost (which depends on the shape of the network) to the contraction of the network without labels. The derivatives with respect to the parameters in each tensor can be computed as follows: first a forward pass which contracts the network is performed, while saving intermediate contraction results (Fig. 8a-f). Then a backward pass computes the derivatives with respect to tensors in each layers separated by copy operations (Fig. 8g-i). In the last layer of a generalized tensor network, the derivative with respect to a tensor is simply obtained by contracting the rest of the network with the corresponding tensor removed, just as in a standard tensor network. Once this is done one can compute the derivatives in the previous layer by observing that the copy operation decouple smaller tensor networks. We observe that from the point of view of supervised learning there is no essential difference between SBS and MPS in terms of the optimization algorithms: the cost of optimizing a SBS is only a constant factor (the number of strings) more than that of optimizing a MPS, and this procedure can be straightforwardly parallelized. This is unlike in quantum physics where Monte Carlo sampling is necessary to optimize a SBS.

So far we have not discussed the positivity of the tensor network. Since the elements are taken to be real, it might not be possible to interpret the contracted network as a probability distribution. To avoid this problem and being able to use the previous algorithm, we can replace $p(\mathbf{x}, y) = \text{GTN}(\mathbf{x}, y)$ by $p(\mathbf{x}, y) = |\text{GTN}(\mathbf{x}, y)|^2$ (which corresponds to a Born machine as defined in Refs. [58, 59]) or $p(\mathbf{x}, y) = \exp(\text{GTN}(\mathbf{x}, y))$. In practice, we find that a suitable initialization of the network for a snake-SBS is to take tensors close to the identity for all possible value of the input leg (which corresponds to having identity matrices in a MPS) and data normalized between 0 and 1. This leads to an initial network that is positive and we find that the network is still positive on all test data after learning. In this case, the original network, the network squared or the exponential of the network give the same classification predictions. Nevertheless we find that learning works better if we choose $p(\mathbf{x}, y) = \exp(\text{GTN}(\mathbf{x}, y))$, which automatically ensures that the resulting distribution is positive, and in the fol-

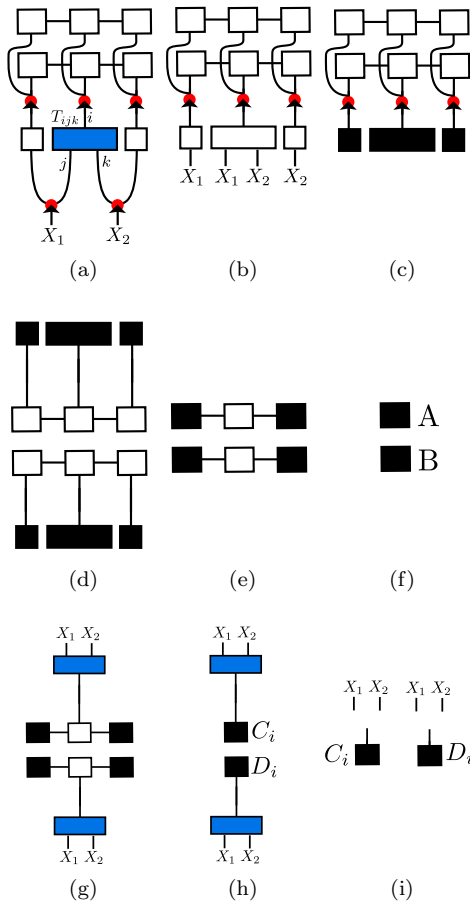


FIG. 8. (a)-(c) Forward pass of contracting an EPS-SBS generalized tensor network. We denote scalar and vectors that are the result of a tensor contraction as black boxes, while other tensors are denoted as empty boxes. The result is a scalar $A \times B$. (d)-(f) We compute as an example the derivative with respect to the tensor T_{ijk} denoted in blue in (a). The computation can start from stage (d), obtained during the forward propagation. Remaining additional tensors are contracted until we are left with the log-derivative, equal to $\partial \log \text{GTN}(X_1, X_2) / \partial T_{ijk} = \delta_{X_1=j} \delta_{X_2=k} (C_i + D_i) / (AB)$.

lowing we always use this construction. This choice can be interpreted as a softmax function after the tensor network's output. In this case the log-derivatives of the tensor network in the derivative of the cost function have to be replaced by the derivatives of the tensor network. To further regularize the tensor network, we adopt the procedure suggested in Ref. [16] to randomly drop tensor elements to 0 with probability δ during training.

So far we have constructed tensor networks which, when an input and a label is given, have no open legs. We can also construct networks with open legs and use tensor networks in combination with other machine learning techniques. In this case the tensor network maps the input to a tensor which can for example be used as input in a neural network. In the case of EPS where each tensor over overlapping plaquettes has an open leg, an input

is mapped to a tensor with an extra dimension as output. This is similar to the role of convolutional filters in a CNN, with the difference that EPS encode all possible filters on discrete inputs. The simplest way to combine EPS with other neural networks is to place a linear classifier on top of the EPS (Fig. 7c). The backpropagation algorithm used to compute derivatives of the neural network is in this case combined with the algorithm for computing derivatives of a tensor network, and the joint network can be optimized using stochastic gradient descent.

IV. LEARNING FEATURE VECTORS OF DATA

In the previous discussion we have always considered discrete input data. In practice, one may want to apply these techniques to real data. In this section we explore several strategies that can be used for this purpose. We suggest to learn relevant tensor features as part of the tensor network and discuss how tensor features can also be learned as part of a deep learning architectures which combines a neural network extracting features with a tensor network.

A naive way of applying tensor networks with real data would be to discretize data or use its binary representation. This is not a suitable approach, because that would amount to increasing the size of the data a lot, rendering learning very slow, and would also lead to big tensor networks which would be prone to overfitting. Another approach, as suggested in Ref. [15], is to map the real data to a higher dimensional feature space. Each variable is first independently mapped to a vector of length at least two and these vectors are then contracted with the open legs of the tensor network (Fig. 9a). Choices of feature maps that have been used in Refs. [15, 16, 45, 46] include

$$x \rightarrow \begin{pmatrix} 1 \\ x \end{pmatrix} \text{ or } \begin{pmatrix} \cos(\frac{\pi}{2}x) \\ \sin(\frac{\pi}{2}x) \end{pmatrix}, \quad (25)$$

and generalizations to higher dimensions. A choice which is suitable with our algorithm, assuming that the data is normalized between 0 and 1, is to use

$$x \rightarrow \begin{pmatrix} \cos^2(\frac{\pi}{2}x) \\ \sin^2(\frac{\pi}{2}x) \end{pmatrix}, \quad (26)$$

because this ensures that the vectors are positive and the normalization prevents numerical instabilities.

These choices however put severe limitations to the functions that can be learned. Indeed, the dataset with just two variables presented in Fig. 10a cannot be separated by a MPS of bond dimension 2 with one of these feature choices, since the boundary decision will be a polynomial of degree two of the features. Nevertheless, a different feature choice could distinguish the two classes, even with bond dimension 2. We therefore suggest to learn the appropriate features as part of the learning algorithm. This can be done by parametrizing the feature

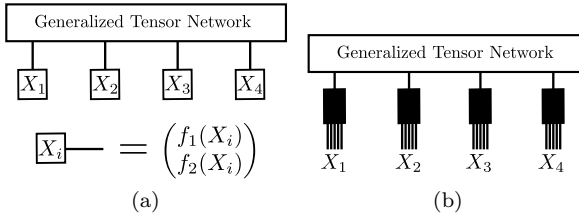


FIG. 9. (a) Real inputs X_i are mapped to a feature vector (here with length two). This vector can then be used as input to a generalized tensor network by contracting it with the open legs of the generalized tensor network. (b) Feature tensors can compress the discretized representation of the inputs X_i to a smaller dimensional space. These tensors can share weights and can be learned as part of the tensor network.

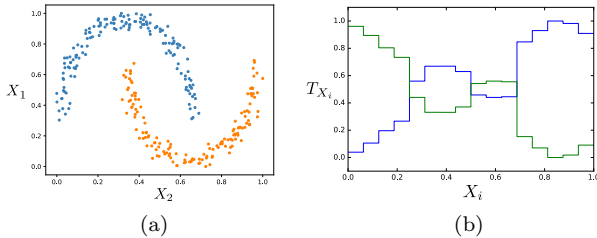


FIG. 10. (a) Dataset with two features X_1 and X_2 and two classes (depicted in different colors) that cannot be learned by a MPS of bond dimension 2 with features in Eq. (26). (b) Two normalized features learned by a tensor while classifying the previous dataset with a MPS of bond dimension 2. The features have been discretized in 16 intervals. Using this choice of features the MPS can classify the dataset perfectly.

functions and learning them at the same time as the rest of the network. To be able to use a purely tensor network algorithm, we can parametrize these functions using a tensor network. In the simplest case, we discretize the real data and use a tensor to compress the large dimensional input into a smaller dimensional vector of suitable length. This tensor can be learned as part of the whole tensor network and prevents the size of the rest of the tensor network to increase when the discretization size changes. The feature tensor can be the same for all variables, for example image pixels, but can be different in the case where the variables are of different nature. Using this procedure, a MPS of bond dimension 2 is able to get perfect accuracy on the dataset presented in Fig. 10a. The two features that the network has learned are presented in Fig. 10b. We note that starting from random features on more complex datasets makes learning difficult, but the feature tensor can be pretrained using a linear classifier, before being trained with the rest of the network.

In comparison, we also show in Fig. 11b the features learned while classifying MNIST with greyscale pixels and a snake-SBS (see section V). These features are not very different from the choice in Eq. 26 (Fig. 11a), and we could not distinguish performance with this choice or

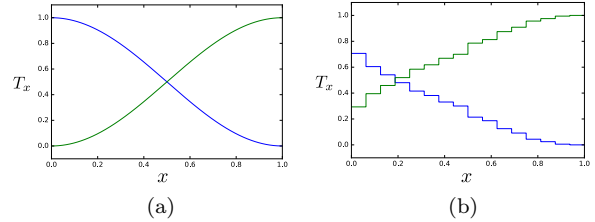


FIG. 11. (a) Choice of two features in Eq. (26) for an input taking real values between 0 and 1. (b) Two normalized features learned by a tensor with output dimension 2 combined with a snake-SBS classifying the MNIST dataset. The input features x are the greyscale value of pixels, normalized between 0 and 1 and discretized in 16 intervals.

with learned features on this dataset. We expect however that this procedure will be necessary for more complex datasets which are not easily approximated by a binary function. Moreover the size of the feature vector provides a regularization of the model, and higher sizes might be necessary for more complex datasets. More generally this tensor could be itself represented with a small tensor network, to prevent the number of parameters to increase too much with a very small discretization interval. It is interesting to note that the features learned in our examples are almost continuous even if we use smaller discretization intervals. This means that two real inputs that are close to each other will lead to the same predictions by the network, a property which is in general not true if we simply discretize the inputs and use a larger tensor network. Our approach of learning the features as part of the tensor network may be especially relevant in the context of quantum machine learning, where the tensor network is replaced by a quantum circuit and it might be suitable to have the full network as part of the same quantum machine learning architecture.

As an alternative way of choosing the features, we can combine the feature choice with other machine learning techniques. If the input data represents images, it is a natural choice to use Convolutional Neural Networks as feature extractors, since these have been highly successful for image classification. CNN consist in convolution filters, which use convolutional kernels to transform an image into a set of filtered images, and pooling layers which downsize the images (Fig. 12). The different filters can be seen as different features of the corresponding pixel or region of the image and preserve locality. Therefore it is natural to consider the vector of applied filters associated with each location in the image as a feature vector that can be used in conjunction with generalized tensor networks. The CNN and the tensor network can be trained together, since the derivatives of the tensor network can be used in the backpropagation algorithm which computes the gradient of the cost function.

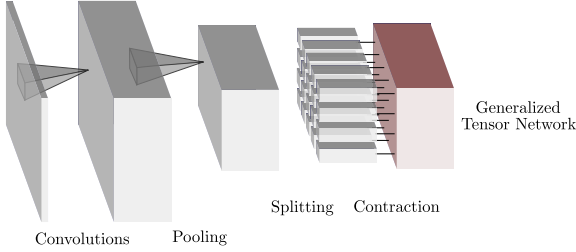


FIG. 12. Using convolutional Neural Networks as feature extractors from real data: the output of the CNN is seen as an image with a third dimension collecting the different features. For each pixel of this image, the vector of features is contracted with the open legs of a tensor network.

V. NUMERICAL EXPERIMENTS

We test the generalized tensor network approach on the task of image classification, where a natural two-dimensional geometry that can be reflected in the architecture of the tensor network is present, as well as on the task of urban sound recognition, where the time dimension provides a one-dimensional geometry.

A. Image classification

We first consider the MNIST dataset[48], which consists of 28×28 greyscale images of digits. There are 10 classes and we adopt a multiclass classification procedure in which one tensor of the tensor network is parametrized by the ten possible labels. The original training set is split into training and validation sets of 55000 and 5000 examples and the performance of the different models is evaluated on the test set of 10000 examples. We consider the following generalized tensor networks: a snake-SBS with 4 strings (Fig. 5b), a 2D-SBS (Fig. 5a), an EPS with a 2×2 translational-invariant plaquette combined with a linear classifier, (Fig. 7c), an EPS-SBS with translational-invariant plaquette combined with a snake-SBS (Fig. 6) and a CNN-snake-SBS which uses a 1-layer CNN as input features (Fig. 12). The CNN considered here uses a convolutional layer applying $6 \times 5 \times 5$ filters (stride 1) with ReLU activation function and a pooling layer performing max pooling with a 2×2 filter. All other networks use the choice of features presented in Eq. (26) and the greyscale values are normalized between 0 and 1. We compare the performance of these networks with a MPS and a RBM (the number of hidden units of 250, 500, 750 or 1000 is taken as a hyperparameter). All networks use a batch size of 20 examples and hyperparameters such as the learning rate α , the regularization rate δ and number of iterations over the training set are determined through a grid search while evaluating the performance on the validation set. Best performance is typically achieved with $\alpha = 10^{-4}$, $\delta = 0.95$ and a hun-

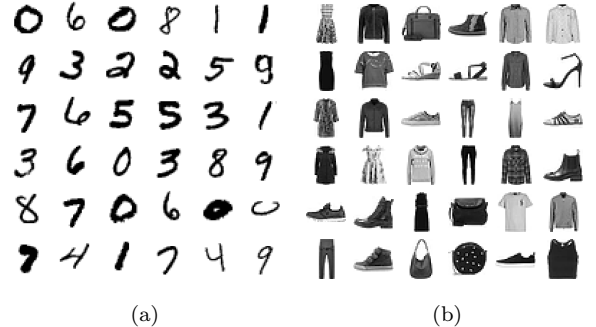


FIG. 13. Examples of images from the MNIST (a) and fashion MNIST (b) dataset.

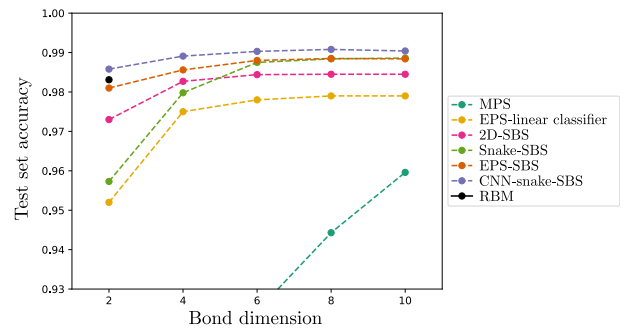


FIG. 14. Test set accuracy of different generalized tensor networks on the MNIST dataset.

dred iterations.

The test set accuracy, presented in Fig. 14, shows that even with a very small bond dimension generalized tensor network are able to accurately classify the dataset. Their performance is significantly better than that of a tree tensor network[46] or a MPS trained in frequency space[45], and while a MPS can also achieve 99.03% accuracy with a bond dimension of 120 [15], the cost of optimizing very large tensors has prohibited the use of this method for larger problems so far. The snake-SBS with bond dimension larger than 6 has also better performance than a RBM. Since the snake-SBS provides an interpolation between RBM and MPS, the choice of number of strings and geometry can be seen as additional parameters which could be tuned further to improve over the performance of both methods. All networks have a training set accuracy very close to 100% when the bond dimension is larger than 6, and we expect that better regularization techniques or network architectures have to be developed to significantly increase the test set performances obtained here. We also optimized a snake-SBS with positive elements (by parametrizing each element in a tensor as the exponential of the new parameters), which is a graphical model. Using the same algorithm, we were not able to achieve better performance than 93% classification accuracy with bond dimensions up to 10. This shows that while having a structure closely related to

graphical models, tensor networks may provide different advantages.

Method	Accuracy
Support Vector Machine	84.1%
EPS + linear classifier	86.3%
Multilayer perceptron	87.7%
EPS-SBS	88.6%
Snake-SBS	89.2%
AlexNet	89.9%
CNN-snake-SBS	92.3%
GoogLeNet	93.7%

TABLE I. Test set accuracy of generalized tensor networks and other approaches[47] on the fashion MNIST dataset.

We then turn to the fashion MNIST dataset[47], consisting of 28×28 greyscale images of clothes. While having the same size as the original MNIST dataset, it is significantly harder to classify. We report the best accuracy obtained with different generalized tensor networks with bond dimension up to 10 in Table I. It is found that these networks are competitive with other approaches such as Support Vector Machines, AlexNet and GoogLeNet Convolutional Neural Networks or a multilayer perceptron neural network, which is encouraging considering the potential improvements in terms of network architecture or training algorithms.

B. Environmental sound classification

So far we have considered black and white images, but it is also interesting to study how generalized tensor networks could be used for other types of data. In the following we consider the task of classifying environmental sounds. The UrbanSound8K dataset[60] is a collection of 8732 audio clips (4s or less) divided into 10 classes of urban sounds: air conditioner, car horn, children playing, dog barking, drilling, engine idling, gun shot, jackhammer, siren and street music. The dataset is divided into 10 folds and we use folds 1-9 for training and fold 10 for testing. The one-dimensional structure of sounds allows us to compare MPS and SBS with the same 1D string geometry. Preprocessing of the data takes place as follows : clips shorter than 4s are repeated to reach a fixed length of 4s. The first 13 Mel-frequency cepstral coefficients (MFCCs) are extracted for each clip (sampled at 22050Hz) using a window size of 2048 and hop length of 512, resulting in a sequence of length 173 and dimension 13 (Fig. 15). The corresponding 13-dimensional vectors are used as input feature vectors for the tensor network, and the time dimension of the sequence corresponds to the 1-dimensional structure of the MPS, or the strings of the SBS. Note that we do not perform any data augmentation nor split the training examples to enlarge the size

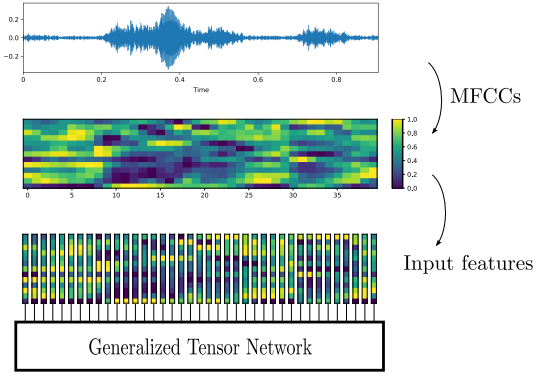


FIG. 15. From the raw audio signal, Mel-frequency cepstral coefficients (MFCCs) are extracted over short overlapping windows, resulting in a sequence of high dimensional vectors. These vectors are taken as input to a generalized tensor network.

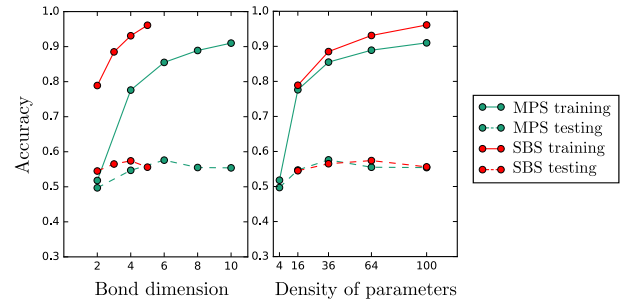


FIG. 16. Training and testing accuracy of a MPS and a SBS with 4 strings on the UrbanSound8K dataset. The density of parameters is the total number of parameters divided by 174 (the length of the strings).

of the dataset set, since we are interested in comparing MPS and SBS, rather than achieving the best possible accuracy on this dataset. The training and testing accuracies are reported in Fig. 16 for a MPS with bond dimension up to 10 and a SBS with 4 strings and bond dimension up to 5. Since we are interested in comparing the expressivity of the different networks, no regularization is used and training is performed until the training accuracy does not improve anymore. Note that a MPS with bond dimension D has as many variational parameters as a SBS with 4 strings and bond dimension $D/2$.

We observe that the SBS has slightly higher training accuracy than a MPS with larger bond dimension and the same number of parameters. The test set performance is not significantly different between the different architectures and in both cases we find that a lot of overfitting has taken place, which is not surprising given the small number of training examples. Higher accuracies have been reported with other methods on the same dataset. For example Convolutional Neural Networks can reach above 70% test set accuracy[49], but use much more input features and rely on data augmentation. Nevertheless our results show that SBS should also be considered along

with MPS when considering one-dimensional data, and may be applied in other settings such as natural language processing[61, 62].

VI. CONCLUSION

We have introduced generalized tensor networks, which enlarge the class of tensor networks by introducing a reuse of information taking the form of a copy operation of tensor elements. The resulting networks include graphical models as special cases and we have discussed the strong relations that exist between particular graphical models and tensor network structures, such as restricted Boltzmann machines and String-Bond States. We provided an algorithm to train these models to perform a supervised learning task and discussed several strategies to use tensor networks in conjunction with real-valued data. We showed that generalized tensor networks that can be contracted exactly can perform accurate image classification with much smaller bond dimension than regular tensor networks, that they can be used in other settings such as sound recognition and that they can be combined with neural-network architectures. Tensor networks can also be seen as a tool to simulate quantum circuits, and there

is much research trying to understand how quantum circuits can be used in machine learning. Quantum circuits corresponding to MPS or tree tensor networks have been studied in the context of quantum machine learning[26]. To implement the function corresponding to a SBS with classical input data one needs to copy the input data and implement each MPS in a similar way. More generally one can expand the generalized tensor network with copy operations as a large tree tensor network in which several tensors are the same and the inputs are copied, and such a tensor network can also be implemented as a quantum circuit. This shows that quantum machine learning circuits should take as input several copies of each data input and not just a single one. Generalized tensor networks which originate from the classical simulation of quantum states may thus serve as a testing and benchmarking platform of near-term quantum machine learning architectures.

ACKNOWLEDGMENTS

We would like to thank Shi-ju Ran, Yoav Levine and Miles Stoudenmire for discussions, as well as Vedran Dunjko for a careful reading of the paper and helpful comments. This work was supported by the ERC grant QUENOCOBA, ERC-2016-ADG (Grant no. 742102). NP acknowledges financial support from ExQM.

[1] R. Orús, “A practical introduction to tensor networks: Matrix product states and projected entangled pair states,” *Annals of Physics* **349**, 117 (2014).

[2] F. Verstraete, V. Murg, and J. Cirac, “Matrix product states, projected entangled pair states, and variational renormalization group methods for quantum spin systems,” *Adv. Phys.* **57**, 143 (2008).

[3] A. Cichocki, N. Lee, I. Oseledets, A.-H. Phan, Q. Zhao, and D. P. Mandic, “Tensor networks for dimensionality reduction and large-scale optimization: Part 1 low-rank tensor decompositions,” *Foundations and Trends in Machine Learning* **9**, 249 (2016).

[4] A. Cichocki, A.-H. Phan, Q. Zhao, N. Lee, I. Oseledets, M. Sugiyama, and D. P. Mandic, “Tensor networks for dimensionality reduction and large-scale optimization: Part 2 applications and future perspectives,” *Foundations and Trends in Machine Learning* **9**, 431 (2017).

[5] A. Novikov, D. Podoprikin, A. Osokin, and D. Vetrov, “Tensorizing neural networks,” arXiv:1509.06569 (2015).

[6] A. Hallam, E. Grant, V. Stojovic, S. Severini, and A. G. Green, “Compact neural networks based on the multiscale entanglement renormalization ansatz,” arXiv:1711.03357 (2017).

[7] R. Yu, S. Zheng, A. Anandkumar, and Y. Yue, “Long-term forecasting using tensor-train RNNs,” arxiv:1711.00073 (2017).

[8] J. Kossaifi, Z. C. Lipton, A. Khanna, T. Furlanello, and A. Anandkumar, “Tensor contraction and regression networks,” arxiv:1707.08308 (2017).

[9] N. Cohen, O. Sharir, and A. Shashua, “On the expressive power of deep learning: a tensor analysis,” in *29th Annual Conf. on Learning Theory* (2016) pp. 698–728.

[10] N. Cohen and A. Shashua, “Inductive bias of deep convolutional networks through pooling geometry,” in *5th International Conference on Learning Representations* (2016).

[11] N. Cohen, O. Sharir, and A. Shashua, “Convolutional rectifier networks as generalized tensor decompositions,” in *33rd International Conference on Machine Learning* (2016) pp. 955–963.

[12] N. Cohen, O. Sharir, Y. Levine, R. Tamari, D. Yakira, and A. Shashua, “Analysis and design of convolutional networks via hierarchical tensor decompositions,” arXiv:1705.02302 (2017).

[13] Y. Levine, D. Yakira, N. Cohen, and A. Shashua, “Deep learning and quantum entanglement: Fundamental connections with implications to network design,” in *6th International Conference on Learning Representations* (2018).

[14] A. Anandkumar, R. Ge, D. Hsu, S. M. Kakade, and M. Telgarsky, “Tensor decompositions for learning latent variable models,” *J. Mach. Learn. Res.* **15**, 2773 (2014).

[15] E. M. Stoudenmire and D. J. Schwab, “Supervised learning with quantum-inspired tensor networks,” *Advances in Neural Information Processing Systems* **29**, 4799 (2016).

[16] A. Novikov, M. Trofimov, and I. Oseledets, “Exponential machines,” arxiv:1605.03795 (2016).

[17] M. Blondel, M. Ishihata, A. Fujino, and N. Ueda, “Polynomial networks and factorization machines: new insights and efficient training algorithms,” in *33rd International Conference on International Conference on Machine Learning* (2018) pp. 850–858.

[18] J. Biamonte, P. Wittek, N. Pancotti, P. Rebentrost, N. Wiebe, and S. Lloyd, “Quantum machine learning,” *Nature* **549**, 195 (2017).

[19] V. Dunjko and H. J. Briegel, “Machine learning and artificial intelligence in the quantum domain: a review of recent progress,” *Reports on Progress in Physics* (2018).

[20] E. Farhi, J. Goldstone, and S. Gutmann, “A quantum approximate optimization algorithm,” arXiv:1411.4028 (2014).

[21] J. R. McClean, J. Romero, R. Babbush, and A. Aspuru-Guzik, “The theory of variational hybrid quantum-classical algorithms,” *New J. of Phys.* **18**, 023023 (2016).

[22] E. Farhi and H. Neven, “Classification with quantum neural networks on near term processors,” arxiv:1802.0600 (2014).

[23] M. Schuld and N. Killoran, “Quantum machine learning in feature hilbert spaces,” arxiv:1803.07128 (2018).

[24] M. Benedetti, D. Garcia-Pintos, Y. Nam, and A. Perdomo-Ortiz, “A generative modeling approach for benchmarking and training shallow quantum circuits,” arxiv:1801.07686 (2018).

[25] K. Mitarai, M. Negoro, M. Kitagawa, and K. Fujii, “Quantum circuit learning,” arXiv:1803.00745 (2018).

[26] W. Huggins, P. Patel, K. B. Whaley, and E. M. Stoudenmire, “Towards quantum machine learning with tensor networks,” arxiv:1803.11537 (2018).

[27] E. Grant, M. Benedetti, S. Cao, A. Hallam, J. Lockhart, V. Stojovic, A. G. Green, and S. Severini, “Hierarchical quantum classifiers,” arXiv:1804.03680 (2018).

[28] A. Critch and J. Morton, “Algebraic geometry of matrix product states,” *SIGMA Symmetry Integrability Geom. Methods Appl.* (2014).

[29] M. Kliesch, D. Gross, and J. Eisert, “Matrix-product operators and states: Np-hardness and undecidability,” *Phys. Rev. Lett.* **113**, 160503 (2014).

[30] J. Chen, S. Cheng, H. Xie, L. Wang, and T. Xiang, “Equivalence of restricted boltzmann machines and tensor network states,” *Phys. Rev. B* **97**, 085104 (2018).

[31] I. Glasser, N. Pancotti, M. August, I. D. Rodriguez, and J. I. Cirac, “Neural-network quantum states, string-bond states, and chiral topological states,” *Phys. Rev. X* **8**, 011006 (2018).

[32] E. Robeva and A. Seigal, “Duality of graphical models and tensor networks,” arXiv:1710.01437 (2017).

[33] K. Fukushima, “Neural network model for a mechanism of pattern recognition unaffected by shift in position - neocognitron,” *Trans. IECE* **J62-A(10)**, 658665 (1979).

[34] Y. LeCun, B. Boser, J. S. Denker, D. Henderson, R. E. Howard, W. Hubbard, and L. D. Jackel, “Back-propagation applied to handwritten zip code recognition,” *Neural Computation* **1(4)**, 541551 (1989).

[35] P. Smolensky, “Information processing in dynamical systems: Foundations of harmony theory,” D. Rumelhart and J. McClelland (Eds.), *Parallel distributed process-* ing, vol. 1, chapter 6, MIT Press (1986).

[36] G. E. Hinton, “Training products of experts by minimizing contrastive divergence,” *Neural Comput.* **14(8)**, 17711800 (2002).

[37] N. Schuch, M. M. Wolf, F. Verstraete, and J. I. Cirac, “Simulation of quantum many-body systems with strings of operators and Monte Carlo tensor contractions,” *Phys. Rev. Lett.* **100**, 040501 (2008).

[38] A. Sfondrini, J. Cerrillo, N. Schuch, and J. I. Cirac, “Simulating two- and three-dimensional frustrated quantum systems with string-bond states,” *Phys. Rev. B* **81**, 214426 (2010).

[39] I. V. Oseledets, “Tensor-train decomposition,” *SIAM Journal on Scientific Computing* **33**, 2295 (2011).

[40] A. Gendiar and T. Nishino, “Latent heat calculation of the three-dimensional $q = 3, 4$, and 5 potts models by the tensor product variational approach,” *Phys. Rev. E* **65**, 046702 (2002).

[41] F. Mezzacapo, N. Schuch, M. Boninsegni, and J. I. Cirac, “Ground-state properties of quantum many-body systems: entangled-plaquette states and variational Monte Carlo,” *New J. Phys.* **11**, 083026 (2009).

[42] H. J. Changlani, J. M. Kinder, C. J. Umrigar, and G. K.-L. Chan, “Approximating strongly correlated wave functions with correlator product states,” *Phys. Rev. B* **80**, 245116 (2009).

[43] Y. Levine, O. Sharir, N. Cohen, and A. Shashua, “Bridging many-body quantum physics and deep learning via tensor networks,” arxiv:1803.09780 (2018).

[44] Z.-Y. Han, J. Wang, H. Fan, L. Wang, and P. Zhang, “Unsupervised generative modeling using matrix product states,” arXiv:1709.01662 (2017).

[45] Y. Liu, X. Zhang, M. Lewenstein, and S.-J. Ran, “Learning architectures based on quantum entanglement: a simple matrix product state algorithm for image recognition,” arXiv:1803.09111 (2018).

[46] D. Liu, S.-J. Ran, P. Wittek, C. Peng, R. B. Garca, G. Su, and M. Lewenstein, “Machine learning by two-dimensional hierarchical tensor networks: A quantum information theoretic perspective on deep architectures,” arXiv:1710.04833 (2017).

[47] H. Xiao, K. Rasul, and R. Vollgraf, “Fashion-MNIST: a novel image dataset for benchmarking machine learning algorithms,” arXiv:1708.07747 (2017).

[48] Y. LeCun, C. Cortes, and C. J. Burges, “MNIST handwritten digit database,” <http://yann.lecun.com/exdb/mnist/> (1998).

[49] K. J. Piczak, “Environmental sound classification with convolutional neural networks,” in *IEEE 25th International Workshop on Machine Learning for Signal Processing* (2015) pp. 1–6.

[50] D. Koller and N. Friedman, *Probabilistic Graphical Models: Principles and Techniques - Adaptive Computation and Machine Learning* (The MIT Press, 2009).

[51] B. J. Frey, “Extending factor graphs so as to unify directed and undirected graphical models,” in *Proceedings of the 19th Conference on Uncertainty in Artificial Intelligence* (2003) pp. 257–264.

[52] Q. Zhao, M. Sugiyama, and A. Cichocki, “Learning efficient tensor representations with ring structure networks,” arXiv:1705.08286 (2018).

[53] J. D. Biamonte, S. R. Clark, and D. Jaksch, “Categorical tensor network states,” *AIP Advances* **1**, 042172 (2011).

- [54] F. Verstraete and J. I. Cirac, “Renormalization algorithms for quantum-many body systems in two and higher dimensions,” arxiv:0407066 (2004).
- [55] D. H. Ackley, G. E. Hinton, and T. J. Sejnowski, “A learning algorithm for Boltzmann machines,” *Cognitive Science* **9**, 147 (1985).
- [56] H. Larochelle and Y. Bengio, “Classification using discriminative restricted boltzmann machines,” in *Proceedings of the 25th international conference on Machine learning* (2008) pp. 536–543.
- [57] H. Larochelle, M. Mandel, R. Pascanu, and Y. Bengio, “Learning algorithms for the classification restricted boltzmann machine,” *Journal of Machine Learning Research* **13**, 643 (2012).
- [58] S. Cheng, J. Chen, and L. Wang, “Information perspective to probabilistic modeling: Boltzmann machines versus born machines,” arXiv:1712.04144 (2017).
- [59] J.-G. Liu and L. Wang, “Differentiable learning of quantum circuit born machine,” arXiv:1804.04168 (2018).
- [60] J. Salamon, C. Jacoby, and J. P. Bello, “A dataset and taxonomy for urban sound research,” in *22nd ACM International Conference on Multimedia (ACM-MM’14)* (Orlando, USA, 2014) pp. 1041–1044.
- [61] V. Pestun and Y. Vlassopoulos, “Tensor network language model,” arXiv:1710.10248 (2017).
- [62] V. Pestun, J. Terilla, and Y. Vlassopoulos, “Language as a matrix product state,” arXiv:1711.01416 (2017).